Biomass Burning and Pollution Aerosol over North America: Organic Components and their influence on Spectral Optical Properties and Humidification Response

A. Clarke[1], C. M[c]Naughton[1], V. Kapustin[1], Y. Shinozuka[1], S. Howell[1], J. Dibb[2], J. Zhou[1], B. Anderson[3], V. Brekhovskikh[1], H. Turner[4], M. Pinkerton[1]

[1]School of Ocean and Earth Science and Technology, University of Hawaii
tclarke@soest.hawaii.edu
[2]Institute for the Study of Earth, Oceans, and Space, University of New Hampshire, Durham, NH, USA, jack.dibb@unh.edu
[3]NASA Langley Research Center, Hampton, VA., b.e.anderson@larc.nasa.gov
[4]University of Alabama, Department of Chemical Engineering, hturner@eng.ua.edu

For Journal of Geophysical Research - Atmospheres

July 1, 2006

Index Terms:
aerosols and particles (0305), aerosols (4801),

Keywords:
pollution, biomass burning, organic carbon, optical properties, humidity growth

Abstract

Thermal analysis of aerosol size distributions provided size resolved volatility up to temperatures of 400^{o}C during extensive flights over North America (NA) for the INTEX/ICARTT experiment in summer 2004. Biomass burning and pollution plumes identified from trace gas measurements were evaluated for their aerosol physio-chemical and optical signatures. Fast measurements of soluble ionic mass and refractory black carbon (BC) mass, inferred from light-absorption, were combined with volatility to identify residual volatile organic carbon (VolatileOC) and refractory organic carbon, RefractoryOC. This approach characterized distinct constituent mass fractions present in biomass burning and pollution plumes. The "non-plume" regional haze exhibited statistical properties reflecting both plume types but was dominated by pollution characteristics near the surface and biomass burning aloft.

VolatileOC included most water-soluble organic carbon. RefractoryOC dominated the enhanced shortwave absorption in plumes from Alaskan and Canadian forest fires. The RefractoryOC mass absorption efficiency was about 0.51 m^2g^{-1} at 470 nm and 0.16 m^2g^{-1} at 530nm. Biomass burning, pollution and dust aerosol could be stratified by their combined spectral scattering and absorption properties. Concurrent measurements of the humidity dependence of scattering [f(RH)] found the VolatileOC component to be only weakly hygroscopic resulting in a general decrease of overall f(RH) with increasing OC mass fractions. Under ambient humidity conditions, the systematic relations between physio-chemical properties and f(RH) lead to a reduced variability in the single scattering albedo and a simple dependency on the absorption per unit dry mass for these plume types that may be used to challenge modeled optical properties.

1.0 Introduction

The importance of aerosol physical, chemical and optical properties and their role in regional and global climate forcing is well recognized. Yet there remains considerable uncertainty about the contribution of both natural and anthropogenic aerosols to their overall radiative effects [*Bates et al.*, 2006]. Some of this uncertainty is due to the complex and varied properties of organic aerosols and more information on the contribution of OC to aerosol physio-chemistry is needed in order to better model their optical properties [*Kanakidou et al.*, 2004]. Properties of key significance from a climate and radiative perspective are the size distribution, light scattering and light absorbing properties, and the hygroscopic properties that control the uptake of water, ambient aerosol optical properties and activation in cloud. The extent to which organic aerosol are internally or externally mixed with other aerosol types is also an important determination. Given the thousands of organic species and their diverse characteristics, a means for generalizing relevant properties is desirable. One commonly identified grouping is the water soluble organic carbon (WSOC) species recently measured aboard research aircraft [*Weber et al.*, 2001]. The remaining water insoluble components can be expected to have physiochemical and optical properties distinct from the WSOC.

One optically important characteristic is the particle light absorption coefficient, σ_{ap}. There is a long history of measuring light absorbing carbon (LAC) and black carbon (BC), often associated with soot; and yet significant uncertainties remain and differences exist in fundamental properties like the mass absorption coefficient (MAE) or refractive index and best ways to report them [*Bond and Bergstrom*, 2006]. The recognition that organic carbon (OC) aerosol can absorb appreciably, particularly at shorter wavelengths [*Kirchstetter et al.*, 2004], has refocused attention on light absorbing properties of this so-called "brown carbon" and the need for multi-wavelength measurements [*Andreae and Gelencser*, 2006]. Measurements of MAE for OC aerosol from typical sources are rare but provide an important tool for models that carry OC mass and use it to estimate aerosol optical effects.

Recently, so called Humic Like Substances (HULIS) have been suggested as a major component of absorbing OC. Humic substances include fulvic acid (water soluble), humic acid (base soluble) and humin (insoluble) components [*Graber and Rudich*, 2006]. HULIS also includes both water soluble and insoluble fractions. However, most studies have focused upon the water soluble fraction or fulvic acid component and not the humic acid or insoluble humin component that is more absorbing in the shorter wavelengths [*Graber and Rudich*, 2006]. These authors also note that transformation of OC components and types can occur in the atmosphere over time and considerable uncertainties exist regarding the various sources, transformations and properties of both soluble and insoluble components.

The water uptake by aerosol must be quantified to correctly calculate or model optical effects under actual atmospheric conditions. Recent evaluations of aerosol humidity-dependent growth have recognized the influence of OC in suppressing aerosol growth compared to that of common ionic species alone [*Quinn et al.*, 2005]. Although OC may suppress aerosol growth, the presence of WSOC may enhance the nucleating properties of some insoluble aerosols (such as dust) and making them more effective

cloud condensation nuclei [*Mayol-Bracero et al.*, 2002b]. Hence, OC properties can influence both the direct and indirect radiative effects of aerosol.

Here we demonstrate the application of aerosol volatility, in conjunction with measurements of ions and inferred BC, to establish the volatile and refractory components aerosol OC at 400^{o}C over North America during INTEX-A. An overview of INTEX-A is presented elsewhere [*Singh et al.*, this issue, submitted]. We will demonstrate that the volatile component appears to be dominated by WSOC while the refractory OC is primarily responsible for enhanced absorption at shorter wavelengths relative to BC. This data will be used to establish the MAE for the non-BC component of BB plumes. Statistically robust differences in the mass fractions present in pollution and biomass plumes will be related to their different hygroscopicity as well as spectral signatures associated with their absorbing and scattering properties.

2.0 Aircraft Measurements

2.1 Aircraft Inlet Sampling Performance

During INTEX-A the University of Hawaii (UH) solid diffuser inlet was used to sample in-situ aerosol size distributions and optical properties aboard the NASA DC-8. Aerosol bulk-chemistry filter samples were measured behind the University of New Hampshire (UNH) solid diffuser inlet. Inlet intercomparisons during the 2003 DC-8 Inlet Comparison Experiment (DICE) demonstrated that the UH and UNH inlets perform nearly identically while sampling both supermicrometer sea salt at high (80-95%) relative humidity and supermicrometer mineral dust in desert environments. Comparisons with ground based instrumentation show that the UH and UNH inlets and transport system pass particles with geometric equivalent diameters (D_g) of 3.0 μm and 2.6 μm (for ρ=2.6 g cm^{-3}) with better than 50% efficiency [M^{c}Naughton et al., submitted 2006]. Because aerosol optical properties are typically dominated by smaller particle sizes the INTEX-A DC-8 aerosol data set can reliably address both the direct and indirect effects of aerosols in the ambient atmospheric environment.

2.2 Thermally Resolved Aerosol Size Distributions

Before size distributions were measured, the sample air stream was mixed with an equal flow of dessicated filtered air. This technique minimizes size variability due to water uptake and uncertainties associated with refractive index effects. A modified PMS[1] laser optical particle counter (OPC) was used to measure the dry (RH < 30%), optically effective aerosol size distribution between 0.1 μm and 10 μm every 3 seconds [*Clarke et al.*, 2004]. The OPC is calibrated before during and after deployment using a combination of NIST[2] traceable polystyrene microspheres (Duke Scientific) , silica microspheres, and borosilicate glass microspheres . The He-Ne OPC laser operates at 633 nm and detects light scattered by individual particles over 35 – 145 degrees. Since the OPC measures optically effective sizes (D_{oe}) directly it is well suited to modeling

[1] Particle Measurement Systems, Boulder, Colorado
[2] National Institute of Standards and Technology

aerosol optical properties. Total and submicrometer scattering calculations from the size distributions compared to measured scattering values has an r^2 statistics of better than 0.95 [*Shinozuka et al.*, submitted 2006].

The OPC operates in series with a newly redesigned thermo-optical aerosol discriminator (TOAD). The design is based on [*Clarke*, 1991] but includes an additional temperature channel at 400°C. During horizontal flight legs the TOAD cycles between temperature channels every 30 seconds. This results in thermo-optical characterization of the optically effective size range every 2 minutes. During vertical profiles the OPC does not cycle between temperatures. At a nominal DC-8 ascent/descent rate of 450 m min^{-1} this results in vertical resolution of statistically-robust individual submicrometer aerosol size distributions over 25 meter intervals. Larger particle sizes require averaging due to lower count statistics.

Aerosol chemistry was also measured on filter samples using ion-chromatography as described by *Dibb et al.* . Filter samples were typically exposed for 5-10 min below 6km and somewhat longer aloft and generally analyzed within 24 hours. These data are essential to link measured volatility and aerosol chemistry to its optical effects in the atmosphere. This is due to the dependency of light scattering on ambient humidity as a result of the uptake of water by soluble constituents. Such data is required in order to interpret optical measurements (e.g. satellite retrievals) in terms of the chemical components that give rise to them. Understanding this variability requires merging both soluble and insoluble aerosol components with the measured chemistry and the f(RH) measurements described below.

2.3 Aerosol Optical Properties and f(RH)

Total and submicrometer aerosol scattering ($\sigma_{sp,\,tot}$, $\sigma_{sp,\,sub}$) is measured using two TSI model 3563 3-λ integrating nephelometers [*Anderson et al.*, 1996; *Heintzenberg and Charlson*, 1996] corrected according to [*Anderson and Ogren*, 1998]. The submicrometer TSI nephelometer employs a 1-μm aerodynamic impactor maintained at 30 lpm using an Alicat Scientific volumetric flow controller. Sample air residence time inside the nephelometers is less than 10 seconds and the instrument relative humidity (RH) is typically less than 30%. Two single-wavelength (λ = 540 nm) Radiance Research model M903 nephelometers are operated in parallel providing a direct measurement of the increase in light scattering as a function of relative humidity, f(RH) [*Howell et al.*, 2006a]. The humidified nephelometer is operated at 80% RH while the dry nephelometer RH was maintained below 40%. Temperature and relative humidity were measured using Vaisala RH & T sensors[3]. These sensors were embedded directly in the RRNeph sample outlet without their protective sheath to improve response time. This measurement of f(RH) provides a two point measurement that can be fit using to express the growth response, γ, of the scattering, σ, using Eqn. 1.

[3] Manufacturer stated accuracy +/-2% RH and +/- 0.1°C.

$$\sigma_{wet} = \sigma_{dry} \cdot \left[\frac{\left(1 - \frac{RH_{dry}}{100}\right)}{\left(1 - \frac{RH_{wet}}{100}\right)} \right]^{\gamma} \qquad \text{Eqn. 1}$$

During INTEX-A a prototype 3-λ Radiance Research particle soot absorption photometer (PSAP) was provided by Dr. David Covert (University of Washington) to measure aerosol light absorption at 470, 530, 660 nm wavelengths. The data shown here are based upon calibration and corrections for this new instrument reported elsewhere [*Virkkula et al.*, 2005]. At the relatively high single scatter albedos (SSA) and low PSAP filter loadings seen in INTEX-A, the results are roughly 25% lower than the correction scheme used in the past for single wavelength PSAP's [*Bond et al.*, 1999]. The reasons for the discrepancy are not clear; [*Virkkula et al.*, 2005]suggest that their use of fresh soot from a flame rather than nigrosin dye may be responsible. Neither particle type is representative of the atmospheric aerosol we sampled, and [*Virkkula et al.*, 2005] did not use particles with SSA>0.9. The high aerosol concentrations, low SSA, rapid filter loading and resulting low filter transmittance values may have also contributed. Additionally, the light source and optical path in the prototype instrument used by Virkkula was significantly different than the unit used in INTEX-A. Calibration results since with a newer instrument do not support the logarithmic transform and are closer value to the algorithm of Bond et. al. 1999 (personal correspondence, D. Covert, unpublished results). Consequently, we believe the absorption values presented here may be a lower limit but this will have little effect on the observations discussed here.

3.0 INTEX-A Plumes

Plumes from western North America biomass burning sources can evolve and mix with continental pollution sources to contribute to regional pollution outflow from North America [*Li et al.*, 2005]. The properties of regional pollution can be expected to reflect the input from both biomass and continental plume types along with other more diffuse sources. Repeated encounters with diverse plumes aloft during INTEX-A [*Singh et al.*, this issue, submitted] provide a statistical characterization of the chemistry, physics and optical properties of these aerosol plume types. Here we characterize all data in terms of biomass burning (BB) plumes and pollution (P) plumes that stand out against a regional background. These plumes have been identified based upon trace gas concentrations. An air mass characterization was carried out for 84 INTEX-A "plumes" as flight leg average values covering a total of ~ 24 hours of flight time. These plumes are characterized by signature species (e.g., CO, O_3, NO_2, SO_2, HCN, C_3H_8, and C_2H_2) that exhibited elevated levels over 95th percentile for the altitude level of the observation.

We began the screening procedure by first establishing the background concentrations of the signature species by dividing the measurements into 1-km altitude bins and creating vertical profiles of each species. A plume encounter was identified when one of the tracer species exceeded the 95th percentile of the measured values (with respect to altitude). Also, in order to facilitate the classification, 10-day back trajectories

were analyzed for each plume, as well as secondary tracer species. Biomass burning plumes were associated with high concentrations of the signature species HCN, CO, and ethyne, and elevated levels of the secondary species: absorption, CH_3CN, and K^+. Pollution plumes were associated with high concentrations of the species: O_3, CO, alkanes, SO_2, NMHC, and ultrafine condensation nuclei (> 3 nm). As defined, some of these plumes will inevitably reflect a mix of plume and non-plume air encountered over a given leg. These are available on the NASA INTEX-A archive (ftp-air.larc.nasa.gov/pub/INTEXA/MERGES/DC8/1_MINUTE/).

The spatial distribution of these plumes is shown as circles for our 60s data collected over eastern NA superimposed on the flight tracks (thin lines, **Figure 1a**). The size of the circles are proportional to the 60 second average scattering values. These plumes are also evident in flight-leg average values averaged over 250 m altitude bins in **Figure 1b** and shown as horizontal lines superimposed upon the grey "non-plume" background. Below 1 km the plumes were exclusively identified as pollution. The total number of BB and P plumes are similar in the 1-3 km altitude, a region that includes most active exchange between the boundary layer and free troposphere. From 3-7 km most plumes identified by the 95th percentile exceedences are biomass burning plumes identified as originating in Alaska and western Canada. At higher altitudes, isolated dilute plumes of either type are present which include deep convection over the continent in summer and some intrusions of stratospheric air.

4.0 Thermal Analysis and Aerosol Carbon

Our thermal treatment produces large changes in the aerosol volume distribution and providing information on the volatility of the aerosol components, state of mixing and the residual refractory component remaining at the highest temperature used. High temperature refractory materials include dust, fly ash, black carbon (BC, soot) and organic species stable at high temperatures. It is now clear that some OC can evolve over a range of temperatures that can overlap those at which BC evolves [*Andreae and Gelencser*, 2006; *Bond and Bergstrom*, 2006; *Mayol-Bracero et al.*, 2002b]. BC may also evolve at different temperatures below 450ºC depending upon origin, state of mixing and aging etc. Moreover these papers (and references therein) discuss at length how some of the aerosol OC is also light absorbing, in addition to aerosol BC, prompting the suggested term light absorbing carbon (LAC) for the possible mixtures of these components. Laboratory samples of two of these absorbing OC components (lignin and humic acid) were shown to have multiple peaked structure in their thermal evolution up to temperatures of 700ºC [*Andreae and Gelencser*, 2006]. Enhanced light absorption at shorter wavelengths is characteristic of these and other HULIS such as those observed in biomass-burning aerosols over the Amazon [*Hoffer et al.*, 2005].

Our measurements use these volatility and absorption properties to characterize BC and OC and its influence upon aerosol measured over North America during INTEX-A. In order to clarify our approach we employ the observations shown in **Figure 2** as reconstructed from thermograms shown in the paper by Kirschtetter et al. [*Kirchstetter et al.*, 2004] and Mayol-Bracero et al. [*Mayol-Bracero et al.*, 2002a]. Kirchstetter at al. show the thermally evolved CO_2 before and after extraction of the samples using acetone

to remove acetone soluble OC. Here we plot the difference (the evolved OC soluble in acetone) measured as thermally evolved CO_2 (relative units) in an oxidizing atmosphere for a sample dominated by biomass burning from South Africa in **Figure 2a** and by aerosol dominated by road-tunnel diesel exhaust in **Figure 2b**. Gaussian fits to the curves associated with the light absorbing BC have been added to reflect the apparent contributions from this component. The peak near 400-500ºC in diesel exhaust cases is primarily associated with the light absorbing BC. Diesel soot is a common LAC that is high in BC and it has been found to combust over a narrow temperature range between 470ºC and 510ºC [*Wittmaack*, 2005]. This is consistent with the main peak for pollution in **Figure 1**. However, there is evidence that mixing with other inorganic species and aerosol aging can catalyze oxidation [*Andreae and Gelencser*, 2006] and shift thermal evolution to lower temperatures by as much as 100ºC [*Novakov and Corrigan*, 1995] in response to the presence of metals such as Na^+ or K^+.

The BC peak in **Figure 2a** is suggested here based upon the most distinct peak location but differencing the acetone treated and untreated data peak temperatures may generate some peaks at temperatures that can be uncertain for the reasons just discussed. Most acid soluble OC typically evolves below 400ºC but it does have a "tail" that extends as high as 600ºC. This behavior is also evident for mixed pollution and biomass burning aerosol collected over the Indian Ocean [*Mayol-Bracero et al.*, 2002a] using a similar technique (**Figure 2c)** and Amazonia [*Mayol-Bracero et al.*, 2002b]. Here the light absorbing BC peak was identified during thermal evolution and is highlighted as a darkened lognormal about 500ºC. The evolved carbon peaks below 400ºC are non-absorbing particulate OC.

These examples in **Figure 2** should only be taken as broadly illustrative of possible OC and BC thermal volatility and its variability. In general there can be multiple peaks of non absorbing particulate OC volatile below 400ºC we will call VolatileOC. Above 400ºC light absorbing BC evolves but may do so at different temperatures that can depend upon sources, composition, state of mixing, trace metals etc. There is also clearly a less absorbing RefractoryOC component that often evolves at temperatures above 400ºC and in a similar temperature range as absorbing BC and is partially soluble in acetone.

5.0 Aerosol Composition and Thermal Volatility

The vertical lines shown in **Figure 2** at 150ºC, 360ºC and 400ºC include temperatures we have previously used in our thermal analysis of volatility [*Clarke et al.*, 2004]. Our size-resolved thermal analysis was originally developed for clean marine regions where sea-salt, sulfates and low mass fractions (ca. 15%) of organic components typically characterize the aerosol [*Clarke*, 1991]. More recently and using fast measurements of soluble ions [*Weber et al.*, 2001] we were able to identify the contribution of volatile ions to our total volatile aerosol assessment [*Clarke et al.*, 2004; *Howell et al.*, 2006b]. The 400ºC temperature was added for INTEX-A to better remove the OC stable at higher temperatures but without removing the BC, as indicated in the prior discussion. Consequently, in this paper the VolatileOC is the inferred OC volatilized at 400ºC and the RefractoryOC is the inferred OC remaining at 400ºC.

The differences in gas phase properties that allowed identification of BB and P plumes (**Figure 1**) is also reflected in differences in aerosol properties including their volatility. **Figure 3** shows examples of the effect of thermal heating on the size distributions for a representative P and BB plume. These include volume distributions observed at about 40ºC, 150ºC, 360ºC and 400ºC. In this paper only the unheated and 400ºC heated volumes will be used. For the remainder of this publication, aerosol mass fractions derived from the thermally resolved size distributions are based on the following assumptions.

- All accumulation mode aerosol is assumed to be internally mixed. This was generally the case as determined using our thermal Tandem Differential Mobility Analyzer (unpublished INTEX-A data) and consistent with our observations in similarly polluted regions after several hours of aging [*Clarke et al.*, 2004].
- The submicrometer OPC data includes most of the aerosol responsible for light scattering, light absorption, BC (soot) soluble ions, for the INTEX-A experiment with the exception of about 5% of the data when substantial coarse particles are present. We assume the OPC volumes are realistic because light scattering calculated from OPC size distributions was found to reproduce measured light scattering to within about 10% [*Shinozuka et al.*, submitted 2006]
- The submicrometer aerosol components volatile below 400ºC include all the measured soluble ions [*Dibb et al.*, 2003] converted to μg m^{-3} and the volatile organic carbon (VolatileOC). We estimate the mass of VolatileOC by subtracting the volume of the ions from the total volatile volume and assigning a density of 1.3 g cm^{-3} for the remaining VolatileOC volume. This is based upon a suggested range of 1.2 to 1.4 g cm^{-3} for organic aerosol [*Stelson*, 1990; *Turpin and Lin*, 2001] and a reported value of 1.4 g cm^{-3} for biomass smoke [*Reid et al.*, 2005]. We made our choice expecting the VolatileOC to be lower than the BC and RefractoryOC in smoke.
- The aerosol volume (mass) remaining at 400ºC includes refractory organic carbon (RefractoryOC) and absorbing black carbon (BC). The BC mass fraction is inferred (InferredBC) based on a nominal mass absorption efficiency (MAE) of 10 m^2g^{-1}. We have argued that a more appropriate value is likely to be 7.5 m^2g^{-1} [*Clarke et al.*, 2004] and consistent with a recent survey of likely values [*Bond and Bergstrom*, 2006]. However, we use the higher value here in order to allow for a possible optical enhancement due to other internally mixed components [*Fuller et al.*, 1999]. As we will demonstrate, the mass of this BC component is small and the uncertainty associated with this choice has little effect on the resulting inferred OC discussed in this paper.
- We use volume based mixing rules with component densities of 1.8 g cm^{-3} for the refractory BC [*Fuller et al.*, 1999] . We are not aware of any density data on RefractoryOC and have arbitrarily used the recent valueof 1.5 g cm^{-3} for bulk HULIS [*Hoffer et al.*, 2004] as we expect RefractoryOC density to be greater than VolatileOC but less than BC.
- We use a representative mean density of ionic components of about 1.75 g cm^{-3} [*McMurry et al.*, 2002; *Stelson*, 1990]. We also assume any potential interaction between mixed components does not influence their effective density.

- RefractoryOC volume is computed as the difference between volume remaining at 400^{o}C and the volume of inferred BC (i.e. area under the black curve in figure 3 less the volume of inferred BC).

In this manner the total accumulation mode mass is broken down into ionic, VolatileOC, RefractoryOC, and BC mass. If coarse dust or fly ash had been a common contributor to the data then additional procedures could be implemented to extract these components based upon their size distributions [*Clarke et al.*, 2004] but this is not included here. We cannot tell fly ash or submicron dust from RefractoryOC, but we have no reason to believe either was important during INTEX-A. We do not include the possible impact of changes in refractive index upon OPC sizes arising due to volatilizing components here.

The results of this procedure for the examples of P and BB size distributions reveal marked differences and are illustrated here as pie charts in **Figure 3** . The inferred P aerosol dry mass is dominated by soluble inorganic ions (79%) with about 16% volatile OC and 4% refractory OC. The estimated BC is only 2% of the mass and supports the argument above that uncertainty in the MAE has little impact on the determination of the other constituents. In the case of BB these inferred mass fractions are quite different. The BB ionic fraction is about a factor of 4 lower than P at 22%. Volatile OC is a factor of 3 higher at 58% and Refractory OC is a factor of 4 higher at 18%. Inferred BC remains a small fraction of the total mass at 3%.

This approach is used to evaluate all of the thermally-resolved size data for which corresponding ionic and BC estimates were available on the DC-8. The results of these assessments were then stratified into BB and P categories based upon the trace gas analysis described earlier. In this fashion, statistically representative composition and properties can be constructed for BB, and P plumes as well as the regional data not characterized as plumes. **Figure 4** shows histograms of the mass fractions of ions, Volatile OC, RefractoryOC, Inferred BC and f(RH) for the BB, P and non-plumes cases for INTEX-A. The differences noted for the two plume cases shown in **Figure 3** are consistent with the differences evident in the campaign histograms although there is clearly some variability within each plume class. This reflects both variability present in plume composition and that of the airmass into which the plumes are mixed. The largest differences in BB and P mass fractions is in the ions that dominate the mass fraction of P plumes. VolatileOC and RefractoryOC together dominate BB plumes. The typical values for BB are similar to mass fractions reported for biomass burning in Africa [*Haywood et al.*, 2003] of 5%BC, 70%OC and 25% inorganic. Visual inspection of the non-plume histograms suggest BB influences were present in approximately 20% of the data, indicating that pollution was the greatest contributor to regional aerosol properties during INTEX-A.

In spite of the large differences in most BB and P mass fractions evident in **Figure 4** the relative components of the carbon mass are less different in BB and P plumes. Both VolatileOC and RefractoryOC can be present in biomass and pollution aerosol but appear much enhanced relative to BC in the former. **Figure 5** provides histograms of mass fractions of the total carbon defined here as the sum of inferred BC mass and volatile OC. The Volatile OC is typically about 90% of Total OC in P vs. about 75% in BB plumes. RefractoryOC is about 30% of Total OC in BB plumes; twice the

value in typical P plumes. Inferred BC remains a few percent of the carbon in both plumes but is typically a larger fraction of the total refractory mass in P plumes due to the lower Refractory OC in these plumes. However, the lower panels show that the inferred BC in pollution plumes tends to be a larger and much more variable fraction of the refractory mass remaining at 400^{o}C compared Inferred BC in the biomass burning plumes.

This characterization of plumes in terms of their inferred OC fractions suggest properties that may be linked to the physiochemical nature of these aerosol types. However, no measurements of organic aerosol components were made aboard the DC-8 and the rare comparisons with surface sites were too short and/or in inhomogeneous conditions such that no direct comparison of our volatility with independent measurements of aerosol OC concentrations were possible. However, the NOAA P-3 did have a rapid measurement of water soluble OC (WSOC) [*Sullivan et al.*, 2004] for flights over the eastern US during the same time period [*Sullivan et al.*, submitted 2006]. In this paper the authors plot their measured WSOC for non-biomass burning sources below 2 km vs. measured CO. As the DC-8 flew in similar regions and for similar times we can compare our inferred VolatileOC vs. measured CO for comparison to the NOAA-P3 WSOC vs. CO plot from Sullivan et al. to explore similarities in their behavior.

In **Figure 6** we plot our VolatileOC against fast CO measured on the DC-8 [*Sachse et al.*, 1987] below 2 km and we include the line fit proposed by *Sullivan et al.* for non-BB data. The fit line has a slope of 0.026 μgC m^{-3} per ppbv and intercept of -2.0 μgC m^{-3} with an r^2=0.54. In order to be consistent with their approach, in **Figure 6a** only we have adjusted our VolatileOC mass (based upon a 1.3 g cm^{-3}) to values based upon their assumed density of 1.0 g cm^{-3} for WSOC. We note that the scatter in the data, the overall data distribution, the grouping of near zero VolatileOC for CO values over 100-150ppbv are virtually identical to the WSOC data as presented in *Sullivan et al.*. We have also added four data points (green stars) to the plot that were reported by these authors (their Table 2) as measurements in BB. Our DC-8 data for P (red), BB (blue) and non-plume cases (grey) clearly show that our BB cases and three of their four stars have a strong and consistent linear relation with CO. These all fall in the upper limit of our data points. The different relation evident for their fourth star was not discussed by the *Sullivan et al.* Also, their data does not show WSOC values measured below about 0.2 μgC m^{-3} while our estimates go negative at times with a common deviation of about 0.5 μgC m^{-3}. This is largely because we are subtracting heated and unheated size distributions that are sampled sequentially and separated by up to 2 minutes (or up to 20 km at DC-8 speeds). At low and variable concentrations this can generate negative differences. However, the magnitude of this difference suggests an overall uncertainty in our measurement approach of about ± 0.7 μgC m^{-3}. Even so, the clear similarity of the relationship between WSOC and CO and that of our VolatileOC to CO strongly suggests that our VolatileOC contains most of the WSOC and may be a useful proxy for WSOC.

Figure 6b shows the result of plotting our Refractory OC against CO for the same data. Refractory OC has a distinct relation to CO for P and BB plumes with about four times as much Refractory OC per CO concentration evident in the latter. Flight legs with encounters of both P and BB plumes (so-called mixed plumes) are elevated relative to P plumes. Because VolatileOC for BB plumes in **Figure 6** appears quantitatively the same as the WSOC in these plumes, this implies the RefractoryOC in BB plumes (**Figure 6b**)

is mostly insoluble OC. This suggests less RefractoryOC is soluble for these BB plumes than found for BB plumes in the Amazon [*Mayol-Bracero et al.*, 2002b]. Given the relatively small amount of RefractoryOC in P plumes compared to VolatileOC it it is not clear to what extent the RefractoryOC is water soluble.

As VolatileOC appears dominated by WSOC and makes up most of the OC we can explore its relation to variability in γ or f(RH), as indicated in **Figure 4.** In **Figure 7a and 7b** we plot γ vs. the volatile organic carbon fraction and the total ion mass fraction for the data we have been considering here. γ shows no clear relation to the volatile OC fraction. Even though VolatileOC is a larger fraction of total mass in BB plumes (**Figure 3**) γ is actually lower for these plumes indicating it is not a significant contributor to f(RH) and hence only weakly hygroscopic. However, γ is strongly related to the ion mass fraction, the background data and some of the BB data. A plot of γ against the OC fraction of accumulation mode mass, Macc, in **Figure 7c**. clearly shows that RefractoryOC and VolatileOC tend to reduce γ as they become a larger fraction of the aerosol mass. This confirms that the relationship found for surface observations downwind of the east coast and our data in Asian outflow [*Quinn et al.*, 2005] also applies generally to the North American aerosol sampled during INTEX-A.

6.0 Spectral Dependence of Absorption and Refractory OC

As noted in the introduction, the light scattering and light absorbing properties of the aerosol and their wavelength dependence are linked to size and composition. The wavelength dependence of absorption (absorption Angström, α_{ap}) and scattering (scattering Angström, α_{sp}) are defined as:

$$\alpha_{ap} = \frac{\ln\left(\sigma_{ap,470}/\sigma_{ap,660}\right)}{\ln\left(660/470\right)} \text{ and } \alpha_{sp} = \frac{\ln\left(\sigma_{sp,450}/\sigma_{sp,700}\right)}{\ln\left(700/450\right)} \quad \text{Eqn. 2 a,b}$$

Figure 8 shows the result of plotting absorption measured at 470nm against absorption at 660nm for all the data discussed here. Clearly the BB plumes show an enhanced absorption in the shorter wavelengths consistent with other measurements on BB aerosol [*Kirchstetter et al.*, 2004]. Histograms of this wavelength dependence for these plumes are also shown for P and BB. The absorption Angström peaks at about 0.75 and is lower than the nominal 1.0 expected for common BC but is in the range of values (0.7 – 1.1) observed elsewhere for pollution aerosol [*Kirchstetter et al.*, 2004]. The absorption Angström for BB peaks near 1.7 and is consistent with the range of 1.2 – 2.2 reported by the same author for African biomass smoke. The non-plume cases clearly show a greater similarity to the P plume wavelength dependence, as was evident in the mass fraction histograms (**Figure 4**).

As discussed in the introduction, this steeper wavelength dependence is related to the enhanced organic fraction in the BB aerosol (**Figure** 4). We can now ask whether it is the volatile or refractory organic carbon species that is most responsible for the steeper wavelength dependence in either plume type. This is evident in **Figure 9a** where

RefractoryOC/TotalOC is plotted against the absorption Angström. As the RefractoryOC fraction of total OC increases the absorption Angström increases indicating a stronger wavelength dependence for this component. As VolatileOC/TotalOC is just (1 – RefractoryOC/TotalOC) the VolatileOC fraction actually would yield a weaker wavelength dependence (not shown). This confirms RefractoryOC is primarily responsible for the enhanced short wave absorption in BB (largest absorption Angström).

7.0 Discussion

The above data indicates that our combined measurements of size-resolved aerosol thermal volatility, estimated BC mass from light absorption and ionic mass provides estimates of VolatileOC and RefractoryOC. Together these OC components were shown to compromise about 30% ±10% of pollution plumes and about 80% ±10% of biomass burning plumes over North America during INTEX-A. VolatileOC was shown to be related to WSOC while RefractoryOC accounts for the enhanced absorption at shorter wavelengths. Both OC components were shown to lead to a suppression of aerosol growth under increasing humidity as their mass fractions increased.

As mentioned in the introduction, HULIS in biomass burning has been recently identified as contributing to enhanced light absorption at shorter wavelengths. Our data reveals that RefractoryOC dominates this enhanced absorption over North America. Hence, the absorption properties of the RefractoryOC component are those that are important to determine. Because the mass of RefractoryOC is distributed over a well defined size range (**Figure 3)**, it is useful to establish the mass absorption efficiency (MAE) of this component. A known MAE allows models to calculate the absorption from the relevant OC mass present in the models.

We estimate the MAE of RefractoryOC by recognizing that the absorption at 660nm is dominated by BC and that OC generally contributes a negligible amount at this wavelength [*Hoffer et al.*, 2005; *Kirchstetter et al.*, 2004]. We can then account for the contribution of the BC component measured at shorter wavelengths by applying the typical wavelength dependence $\lambda^{-0.8}$ found here (**Figure 8 bottom)** for the P plumes dominated by absorbing BC**.** If we assume the BC component present in BB plumes absorbs with this same wavelength dependence then the BC contribution can be estimated for all wavelengths. When subtracted from the total BB absorption measured at 530 nm and 470 nm this leaves the absorption enhancement ($\Delta\sigma_{ap}$). Based upon **Figure 9a** we assume here that this is due to RefractoryOC in BB alone.

The resulting $\Delta\sigma_{ap}$ data for BB plumes on INTEX-A are shown vs. RefractoryOC mass in **Figure 9b.** The linear slope for $\Delta\sigma_{ap}$ vs. RefractoryOC mass defines the MAE at each wavelength. At 470 nm the slope yields a value of 0.51 m^2g^{-1} while at 530 nm it drops to 0.16 m^2g^{-1}. If we had assumed a λ^{-1} dependence for the small particle limit for high absorbing material for BC absorption in BB aerosol we would get MAE values of 0.47 m^2g^{-1} (470nm) and 0.1 m^2g^{-1} (530nm). While these values appear small compared to the MAE for BC, the refractory OC present in BB aerosol is about ten times the mass of BC (**Figure 4**) making RefractoryOC a significant absorber (about 15% of BC) at 530nm and with absorption similar to BC at 450nm. These MAE values are based upon the 3-λ PSAP absorption, OPC volumes and the assumed density of 1.8 g cm^{-3}. While the latter are reasonable we expect their uncertainty could possibly alter these estimates by as much

as 20%. If the 3-λ PSAP measured absorption is as much as 25% low (as mentioned earlier) then these MAE values will be a lower limit. We also note that our Refractory OC is operationally defined based upon the 400º temperature separation discussed earlier. Hence, the actual absorbing OC component may have a mass somewhat larger or smaller than we estimate here depending upon its exact thermal behavior near 400º as well as possible volatility of non-absorbing components near this temperature. Furthermore, although we have treated RefractoryOC here as a separable component from BC, it is likely to be a primary emission that is absorbing and internally mixed with the BC. Hence, it may act to enhance BC absorption and/or "shield" some of the encapsulated BC from the full intensity of incident radiation [*Fuller et al.*, 1999]. Understanding such effects will require careful modeling of the effective absorption of the combined mixture.

The wavelength dependence of scattering is closely coupled to the size distribution. The examples of BB and P plumes shown in **Figure 2** reveal a difference in size for these plume types with the BB plume being larger. Consequently, if this is a typical feature of these sources, then these plume types should be distinguishable not only by their absorption Angström coefficient but also their scattering Angström coefficient. This is evident in **Figure 10a** where these coefficients are plotted against each other and show a clustering of the BB and P cases. The limited number of cases when the absorption Angstrom is below 0 is in part due to low absorption values (a differential measurement) and the influence of variability in pressure and RH, often worse during profiles. This clustering makes sense in terms of the larger size (smaller scattering Angström) and enhanced shortwave absorption (larger absorption Angström) of BB plumes relative to P. However, a portion of the data identified as P data from trace gas assessment appear to be exceptions and are circled in the figure. In **Figure 10b**, the same data is color coded by the measured Ca^{2+} to accumulation mode mass (Macc) volume whenever Ca^{2+} data was available. These points are clearly enhanced in Ca and all occurred during Flight 18 over the Gulf of Mexico in an airmass coming from the south. Enhanced coarse particles and coarse scatting (not shown) and elevated Ca^{2+} indicate the presence of a mixture of mineral dust and pollution. Dust lowers the scattering Angström [*Clarke et al.*, 2004] and has enhanced absorption at short wavelengths that exceed those of RefractoryOC [*Patterson*, 1981]. A greater dust contribution would lower the scattering Angström and enhance the Absorption Angström even more. Hence, the observed behavior of the circled points makes sense and demonstrates the value of these optical spectral signatures for identifying aerosol types and their mixtures. In principle, such measurements through the atmospheric column could partition the relative contribution of mixed plume types. We also note the indication of a gradient in the absorption Angström within the dense P cluster linked to the Ca/Macc ratio that will be the subject of a future paper exploring this approach.

The spectral measurements of absorption and scattering are related to the underlying physiochemistry of the aerosol, as is true of the humidity dependent response of the aerosol light scattering expressed as **γ.** When the Angström coefficients for absorption and scattering are plotted vs. **γ** they exhibit a decreasing and increasing behavior respectively (**Figure 10c)**. Hence, the difference in the value of these two Angström coefficients could provide an estimate of **γ**. If this relationship is common and if these parameters could be reliably sensed remotely then the effective **γ** might also be

retrieved although mixed properties over the ambient column could make this difficult to apply [*Shinozuka et al.*, submitted 2006].

The above considerations of these optical properties, their link to aerosol physiochemistry and the associated f(RH) or γ also impacts the values of the aerosol single scattering albedo, SSA. This is often reported for the measured dry aerosol although it is the ambient "wet" aerosol that is remotely sensed and most important for modeling atmospheric radiative effects. In this data we have seen systematic differences in size, composition and humidity response for the BB and P plumes. Here we show how these systematic differences in size and f(RH) can lead to a reduced variability in SSA under ambient conditions. We examine SSA dependencies here under the assumption that they are little affected by any modification to absorbing properties by water uptake [*Nessler et al.*, 2004].

The mean accumulation mode aerosol size can be expressed as a size parameter defined by the ratio of measured OPC accumulation mode volume (Vacc) to accumulation mode number (Nacc). The larger the integral volume per integral number of particles in the accumulation mode, such as those in **Figure 2**, then the larger the mean diameter becomes. **Figure 11a** shows the dry SSA vs. the aerosol absorption (530nm) and color coded with this size parameter. A strong "rainbow" effect reveals that dry SSA depends strongly on size and not just absorption. The horizontal spread of data points for BB plumes with larger size (blue) shows that SSA is constant for a large range in absorption. This implies that scattering and absorption scale together in these BB plumes while effective particle size remains the same.

In **Figure 11b** we plot dry SSA against the absorption per unit mass of the accumulation mode. This "collapses" the BB data and "tightens" the spread of the data while preserving and enhancing the "rainbow" effect that reveals the size dependence of dry SSA. For a given color (ie. effective size) the increase in absorption per unit mass results in the expected reduction in SSA with the strongest dependency (steepest slope) evident for the smallest sizes (red). The dependency of SSA on size is clear if you consider the range of colors for particles with a particular absorption per mass (say 0.5 m^2 g^{-1}). These exhibit a range of dry SSA from about 0.91 to 0.97 as their Vacc/Nacc, is seen to increase by a factor of about 4 (0.002 $\rightarrow$ 0.01). This implies an effective diameter increase of $4^{1/3}$ or about 1.6. This is consistent with **Figure 2** that shows a volumetric mean diameter of 0.45 μm for the BB case compared to 0.30 μm for the P case, a factor of 1.5. This shift to higher SSA is evident when the accumulation mode SSA is written a $(1+MAE/MSE)^{-1}$ [*Clarke et al.*, 2004] and the aerosol mass scattering efficiency, MSE, changes more rapidly with size than the mass absorption efficiency, MAE. Because the scattering Angström exponent is more conventionally measured and can be sensed remotely as a size indicator (lower values indicating larger sizes) we show the same data color-coded with this parameter in **Figure 11c**. The scattering Angström exponent is not as directly linked to the accumulation mode size distribution as the parameter Vacc/Nacc but shows the same range and rainbow behavior as **Figure 11b**.

All of the plots in **Figure 11a,b,c** are for the dry aerosol. However, we are more interested in the behavior of SSA under ambient conditions, $SSA_{ambient}$. This is shown in **Figure 11d** where we have recalculated the scattering at ambient RH based upon fits (γ) to continuously measured f(RH) on the DC-8. The data have here been colorcoded with the P, BB and non-plume "background" code used elsewhere. This figure also shows that

much of the spread in the SSA data is reduced. If we look at the variation in $SSA_{ambient}$ again at 0.5 m^2 g^{-1} it is now 0.93 to 0.97, about a factor of two reduction in variability for a given absorption per unit mass. Hence, for a given mass and a given absorption, the uncertainty in $SSA_{ambient}$ is about a factor of two less than dry SSA.

This behavior and the greater increase in $SSA_{ambient}$ for smaller sizes with lower dry SSA can be a consequence of several factors. First, for a given composition or humidity dependent diameter change, g(RH), smaller accumulation mode sizes have significantly higher f(RH) or γ [*Howell et al.*, 2006b]. This results in a greater relative scattering increase for the smaller sizes. Second, the largest accumulation mode aerosol in INTEX-A were measured in the BB plumes (**Figure 2**) having the largest OC fraction (**Figure 3)** and the lowest f(RH) or γ. These considerations imply that, for a given absorption per unit mass, $SSA_{ambient}$ increases more relative to SSA_{dry} for the smallest sizes with the largest ion fractions and changes least for the largest sizes with the lowest ion fraction.

Assuming these INTEX-A measurements are generally representative of aerosol over North America, this observation is promising for models that use MSE, MAE, aerosol mass and relative humidity to calculate ambient aerosol extinction and SSA. **Figure 11d** suggests the range of $SSA_{ambient}$ simulated by a model can be constrained by the regressions indicated for P and BB plumes measured. Models that include the absorbing aerosol component and the accumulation mode mass should obtain typical ambient SSA values indicated in the plot for the regressions on the P and BB plumes. The slopes for these fits are not sensitive over this SSA range to the previously mentioned uncertainty in absorption values. The results indicate that, for the same absorption per unit mass, P plumes will have a somewhat lower $SSA_{ambient}$ values than BB plumes.

Conclusion

Thermal volatility of dry size distributions was used in conjunction with concurrent measured ion concentrations, BC mass estimated from light absorption and realistic density values to provide estimates of the OC mass concentration by difference. Heating to 400ºC is effective at separating out a more volatile and refractory organic component. The VolatileOC component's relation to CO was shown to be similar to that for water soluble OC (WSOC) measured on the NOAA P3_B during the same campaign, indicating that these are likely dominated by the same OC species. On the other hand, only RefractoryOC exhibited the short wavelength enhancement in absorption characteristic of biomass burning aerosol.

This rapid in-situ thermal technique appears capable of characterizing the OC mass of the aerosol related fundamental physio-chemical properties. This was of clear value to INTEX-A where OC was a significant contribution to aerosol mass but no aerosol OC measurements were available on the DC-8. Statistically significant differences in mass fractions of ions, VolatileOC, RefractoryOC, and BC were obtained for biomass (BB) and pollution plumes (P) identified by trace gases. These differences also expressed themselves as less growth under increasing humidity for BB plumes due to their larger OC mass fractions. Comparison of plume features with data not exhibiting plume structure or concentrations (regional background) showed that the latter was more

strongly influenced by P and BB emissions below about 2 km. Above that altitude BB plumes had a greater contribution but their occurrence is both seasonal and episodic.

Multiwavelength measurements of absorption and scattering coefficients proved effective at distinguishing BB, P and dust influenced plumes. The absorption Angström coefficient (470-660 nm) for BB plumes had a value centered about 1.7 while that of P plumes was near 0.75. Enhanced shortwave absorption over that expected for BC in BB plumes was a function of RefractoryOC. The slope of this dependency yielded a mass absorption efficiency, MAE, of this component of about 0.51 m^2g^{-1} at 470 nm and dropping to 0.16 m^2g^{-1} at 530nm with an estimated uncertainty of about 20%. For these biomass burning aerosols the fraction of total absorption due to RefractoryOC was comparable in magnitude to BC at 470 nm but on the order of 10% that of BC at 530 nm.

The humidity dependence of light scattering expressed as f(RH) or γ was shown to depend upon composition and size in ways that were linked to spectral optical properties, including the OC component. The difference in the scatting and absorption Angström exponents increased with f(RH), suggest a possible way to estimate f(RH) with remote spectral measurements. Smaller but more absorbing aerosol in pollution were found to exhibit the largest values for f(RH) while the largest biomass burning aerosol exhibited the lowest f(RH). Under ambient RH conditions these properties tended to reduce variability in SSA at ambient RH for a given absorption per unit mass and regressions for P and BB plumes may provide useful constraints upon model values for ambient SSA.

Acknowledgements: We would like to acknowledge support of part of our team through NASA grant NNG04GB39G for this work. We also thank the NASA DC-8 team at NASA's Dryden Flight Research Center, California for their mission support. We extend a special thanks to Dr. David Covert (U. of Washington) for loan of the 3-λ PSAP for this study. We also thank Dr. Glen Sachse (NASA Langley Research Center) for the CO data used here. This is SOEST contribution number ######.

References

Anderson, T., and J. Ogren (1998), Determining aerosol radiative properties using a TSI 3563 integrating nephelometer, *Aerosol Science and Technology*, *29*, 57-69.

Anderson, T.L., D.S. Covert, S.F. Marshall, M. L. Laucks, R.J. Charlson, A.P. Waggoner, J.A. Ogren, R. Caldow, R. Holm, F. Qyant, G. Sem, A. Wiedensohler, N.A. Ahlquist, and T.S. Bates (1996), Performance characteristics of a high-sensitivity, three-wavelength, total scatter/backscatter nephelometer, *Journal of Atmospheric Oceanic Technology*, *13*, 967-986.

Andreae, M.O., and A. Gelencser (2006), Black carbon or brown carbon? The nature of light- absorbing carbonaceous aerosols, *Atmos. Chem. Phys. Discussions*, *6*, 3419-3463.

Bates, T.S., T.L. Anderson, T. Baynard, T. Bond, O. Boucher, G. Carmichael, A. Clarke, C. Erlick, H. Guo, L. Horowitz, S. Howell, S. Kulkarni, H. Maring, A. McComiskey, A. Middlebrook, K. Noone, C.D. O'Dowd, J. Ogren, J. Penner, P.K. Quinn, A.R. Ravishankara, D.L. Savoie, S.E. Schwartz, Y. Shinozuka, Y.

738 Tang, R.J. Weber, and Y. Wu (2006), Aerosol direct radiative effects over the
739 northwest Atlantic, northwest Pacific, and North Indian Oceans: Estimates based
740 on in-situ chemical and optical measurements and chemical transport modeling,
741 *Atmos. Chem. Phys.*, *6*, 1657-1732.
742 Bond, T.C., T.L. Anderson, and D. Campbell (1999), Calibration and intercomparison of
743 filter-based measurements of visible light absorption by aerosols, *Aerosol Science*
744 *and Technology*, *30*, (6), 582-600.
745 Bond, T.C., and R.W. Bergstrom (2006), Light Absorption by Carbonaceous Particles:
746 An Investigative Review, *Aerosol Sci. Technol.*, *40*, (DOI:
747 10,1080/02786820500421521), 27-67.
748 Clarke, A.D. (1991), A Thermo Optic Technique for Insitu Analysis of Size-Resolved
749 Aerosol Physicochemistry, *Atmospheric Environment Part a-General Topics*, *25*,
750 (3-4), 635-644.
751 Clarke, A.D., Y. Shinozuka, V.N. Kapustin, S. Howell, B. Huebert, S. Doherty, T.
752 Anderson, D. Covert, J. Anderson, X. Hua, I. K. G. Moore, C. McNaughton, G.
753 Carmichael, and R. Weber (2004), Size distributions and mixtures of dust and
754 black carbon aerosol in Asian outflow: Physiochemistry and optical properties, *J.*
755 *Geophys. Res.*, *109*, (D15), 1-20, D15S09, doi:10.1029/2003JD004378.
756 Dibb, J.E., R.W. Talbot, E.M. Scheuer, G. Seid, M.A. Avery, and H.B. Singh (2003),
757 Aerosol chemical composition in Asian continental outflow during the TRACE-P
758 campaign: Comparison with PEM-West B, *J. Geophys. Res.*, *108*, (D21), GTE 36-
759 1 - GTE 36-13, 8815, doi:10.1029/2002JD003111.
760 Fuller, K.A., W.C. Malm, and S.M. Kreidenweis (1999), Effects of mixing on extinction
761 by carbonaceous particles, *J. Geophys. Res.*, *104*, (D13), 15941 - 15954,
762 doi:10.1029/1998JD100069.
763 Graber, E.R., and Y. Rudich (2006), Atmospheric HULIS: how humic are they? A
764 comprehensive and critical review, *Atmos. Chem. Phys.*, *6*, 729-753.
765 Haywood, J.M., S.R. Osborne, P.N. Francis, A. Keil, P. Formenti, M.O. Andreae, and
766 P.H. Kaye (2003), The mean physical and optical properties of regional haze
767 dominated by biomass burning aerosol measured from the C-130 aircraft during
768 SAFARI 2000, *J. Geophys. Res.*, *108*, (D13), SAF 9-1 - SAF 9-14, 8473,
769 doi:10.1029/2002JD002226.
770 Heintzenberg, J., and R.J. Charlson (1996), Design and Applications of the Integrating
771 Nephelometer: A Review, *Journal of Atmospheric Oceanic Technology*, *13*, 987-
772 1000.
773 Hoffer, A., A. Gelenscer, P. Guyon, G. Kiss, O. Schmidd, G. Frank, P. Artaxo, and M.O.
774 Andreae (2005), Optical properties of humic-like substances (HULIS) in biomass
775 burning aerosols., *Atmos. Chem. Phys. Discussions*, *5*, 7341-7360.
776 Hoffer, A., G. Kiss, M. Blazsó, and A. Gelencsér (2004), Chemical characterization of
777 humic-like substances (HULIS) formed from a lignin-type precursor in model
778 cloud water, *Geophys. Res. Lett.*, *31*, (6), 1-4, L06115,
779 doi:10.1029/2003GL018962.
780 Howell, S.G., A.D. Clarke, Y. Shinozuka, V. Kapustin, C.S. McNaughton, B.J. Huebert,
781 S.J. Doherty, and T.L. Anderson (2006a), Influence of relative humidity upon
782 pollution and dust during ACE-Asia: Size distributions and implications for

783 optical properties, *Journal of Geophysical Research-Atmospheres*, *111*, D06205,
784 doi:10.1029/2004JD005759.
785 Howell, S.G., A.D. Clarke, Y. Shinozuka, V.N. Kapustin, C.S. McNaughton, S. Doherty,
786 and T. Anderson (2006b), The Influence of relative humidity upon pollution and
787 dust during ACE-Asia: size distributions and implications for optical properties, *J.*
788 *Geophys. Res.*, *111*, (D06205, doi:10.1029/2004JD005759).
789 Kanakidou, M., J.H. Seinfeld, S.N. Pandis, I. Barnes, F.J. Dentener, M.C. Faccini, R.
790 vanDingenen, B. Ervens, A. Nenes, C.J. Nielsen, E. Swietliki, J.P. Putaud, Y.
791 Balkanski, S. Fuzzi, J. Horth, G.K. Moortgat, R. Winterhalter, C. Meyhr, K.
792 Tsigaridis, E. Vignati, E.G. Stephanou, and J. Wilson (2004), Organic aerosol and
793 global climate modeling: a review, *Atmospheric Chemistry and Physics*
794 *Discussions*, *4*, 5855-6024.
795 Kirchstetter, T.W., T. Novakov, and P.V. Hobbs (2004), Evidence that the spectral
796 dependence of light absorption by aerosols is affected by organic carbon, *Jour.*
797 *Geophys. Res.*, *109*, (doi:10.1029/2004JD004999).
798 Li, Q.B., D.J. Jacob, R. Park, Y.X. Wang, C.L. Heald, R. Hudman, R.M. Yantosca, R.V.
799 Martin, and M. Evans (2005), North American pollution outflow and the trapping
800 of convectively lifted pollution by upper-level anticyclone, *Journal of*
801 *Geophysical Research-Atmospheres*, *110*, (D10), -.
802 Mayol-Bracero, O.L., R. Gabriel, M.O. Andreae, T.W. Kirchstetter, T. Novakov, J.
803 Ogren, P. Sheridan, and D.G. Streets (2002a), Carbonaceous aerosols over the
804 Indian Ocean during the Indian Ocean Experiment (INDOEX): Chemical
805 characterization, optical properties, and probable sources, *J. Geophys. Res.*, *107*,
806 (D19), INX2 29-1-INX2 29-21, 8030, doi:10.1029/2000JD000039.
807 Mayol-Bracero, O.L., P. Guyon, B. Graham, G. Roberts, M.O. Andreae, S. Decesari,
808 M.C. Facchini, S. Fuzzi, and P. Artaxo (2002b), Water-soluble organic
809 compounds in biomass burning aerosols over Amazonia 2. Apportionment of the
810 chemical composition and importance of the polyacidic fraction, *J. Geophys. Res.*,
811 *107*, (D20), LBA 59-1-LBA 59-15, 8091, doi:10.1029/2001JD000522.
812 McMurry, P., X. Wang, K. Park, and K. Ehara (2002), Relationships between Mass and
813 Mobility for atmospheric particles: A new technique for measuring particle
814 density, *Aerosol Sci. Technol.*, *36*, 227-238.
815 Nessler, R., E. Wintergartner, and U. Baltensberger (2004), Effect of humidity on aeosol
816 light absorption and its implication for extinction and the single scatter albedo
817 illustrated for a site in the lower free troposphere., *J. Aerosol Sci.*,
818 *doi:10.1016/j/aerosolsci.2004.11.012*.
819 Novakov, T., and C.E. Corrigan (1995), Thermal characterization of biomass smoke
820 particles, *Microchimica Acta*, *119*, (1-2), 156-166.
821 Patterson, E.M. (1981), Optical properties of crustal aerosol: Relation to chemical and
822 physical characteristics, *Jour. Geophys. Res.*, *86*, (C4), 3236-3246.
823 Quinn, P.K., T.S. Bates, T. Baynard, A.D. Clarke, T. Onasch, W.C. Wang, R. M., E.
824 Andrews, C.M. Carrico, D.J. Coffman, and D. Worsnop (2005), Impact of
825 particulate organic matter on the relative humidity dependence of light scattering,
826 *Jour. Geophys. Res.*, *111*, (D04202, doi101029/2005GL024322).

827 Reid, J.S., R. Koppmann, T.F. Eck, and D.P. Eleuterio (2005), A review of biomass
828 burning emissions part II: intensive physical properties of biomass burning
829 particles, *Atmos. Chem. Phys.*, *5*, 799-825.
830 Sachse, G.W., G.F. Hill, L.O. Wade, and M. G. Perry (1987), Fast-response, high-
831 precision carbon monoxide sensor using a tunable diode laser absorption
832 technique, *J. Geophys. Res.,*, *92*, (2071-2081).
833 Shinozuka, Y., A.D. Clarke, S.G. Howell, and J. Zhou (submitted 2006), Aircraft profiles
834 of aerosol microphysics and optical properties over North America: aerosol
835 optical depth and its association with PM2.5 and water uptake, *Jour. Geophys.*
836 *Res.*
837 Singh, H.B., W. Brune, J. Crawford, and D. Jacob (this issue, submitted), Overview of
838 the Summer 2004 Intercontinental Chemical Transport Experiment-North
839 America (INTEX-A).
840 Stelson, A.W. (1990), Urban aerosol refractive index prediction by partial molar
841 approach, *Environ. Sci. Technol.*, *24*, 1676-1679.
842 Sullivan, A., R.E. Peltier, C.A. Brock, J.A. de Gouw, J.S. Holloway, C. Warneke, A.G.
843 Wollny, and R.J. Weber (submitted 2006), Airborne measurments of
844 carbonaceous aerosol soluble in water over northeastern U.S.A. : Method
845 development and an investigation into WSOC sources., *Jour. Geophys. Res.*
846 Sullivan, A.P., R.J. Weber, A.L. Clements, J.R. Turner, M.S. Bae, and J.J. Schauer
847 (2004), A method for on-line measurement of water-soluble organic carbon in
848 ambient aerosol particles: Results from an urban site, *Geophys. Res. Lett.*, *31*,
849 (13), 1-4, L13105, doi:10.1029/2004GL019681.
850 Turpin, B.J., and H.-J. Lin (2001), Species contributions to PM2.5 mass concentrations:
851 Revisiting common assumptions for estimating organic mass,, *Aero. Sci. Tech.*,
852 *35*, 602–610.
853 Virkkula, A., N.C. Ahlquist, D.S. Covert, W.P. Arnott, P.J. Sheridan, P.K. Quinn, and
854 D.J. Coffman (2005), Modification, Calibration and a Field Test of an Instrument
855 for Measuring Light Absorption by Particles, *Aerosol Sci. Technol.*, *39*, (1, DOI:
856 10.1080/027868290901963), 68-83.
857 Weber, R.J., D. Orsini, Y. Daun, Y.N. Lee, P.J. Klotz, and F. Brechtel (2001), A particle-
858 into-liquid collector for rapid measurement of aerosol bulk chemical composition,
859 *Aerosol Science and Technology*, *35*, (3), 718-727.
860 Wittmaack, K. (2005), Combustion characteristics of water-insoluble elemental and
861 organic carbon in size-selected aerosol particles, *Atmos. Chem. Phys.*, *5*, 1905-
862 1913.
863

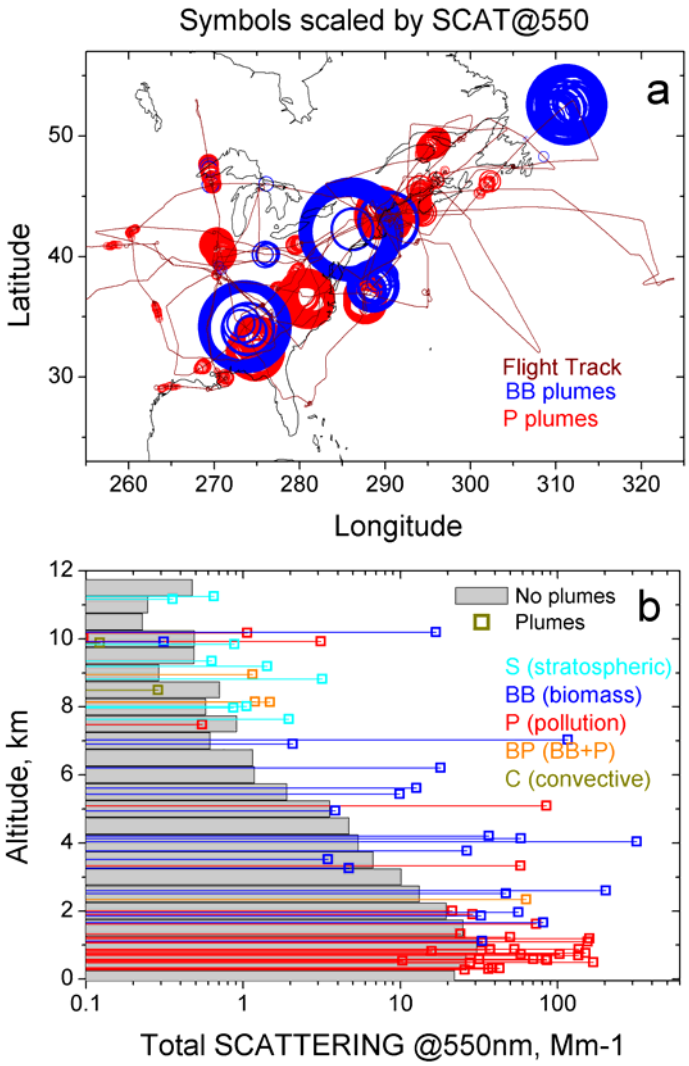

Figure 1. **a)** map of North America showing DC-8 flight routes (thin lines) and plume locations (circles) where diameters are proportional to 60s measured scattering at 530nm. **b)** vertical profile of measured scattering for plume types identified and the average of all non-plume data as a function of altitude during INTEX-A. See text for plume characterization strategy.

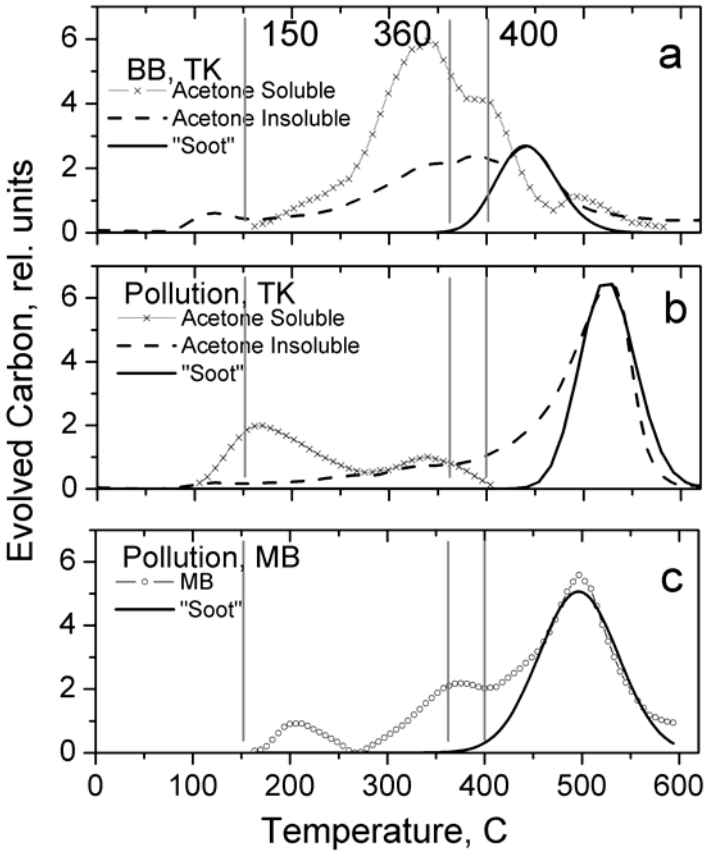

Figure 2. Thermograms of evolved CO_2 in oxygen as adapted from references in text. **a)** thermograms the acetone soluble and acetone insoluble component components for BB sample (African savanna) and apparent absorbing BC peak highlighted near 450C (Kirschtetter, 2001, TK). **b)** same only for tunnel pollution dominated by diesel with BC peak near 520C. **c)** thermogram of pollution/biomass plume from Indian Ocean with concurrent total CO_2 (grey) and CO_2 for the absorption peak (BC) highlighted near 490C (Mayol-Bracero, 2002a, MB). These reveal that OC can evolve at many temperatures including those associated with BC (a) and that the temperature where absorbing BC can evolve can vary with sample type.

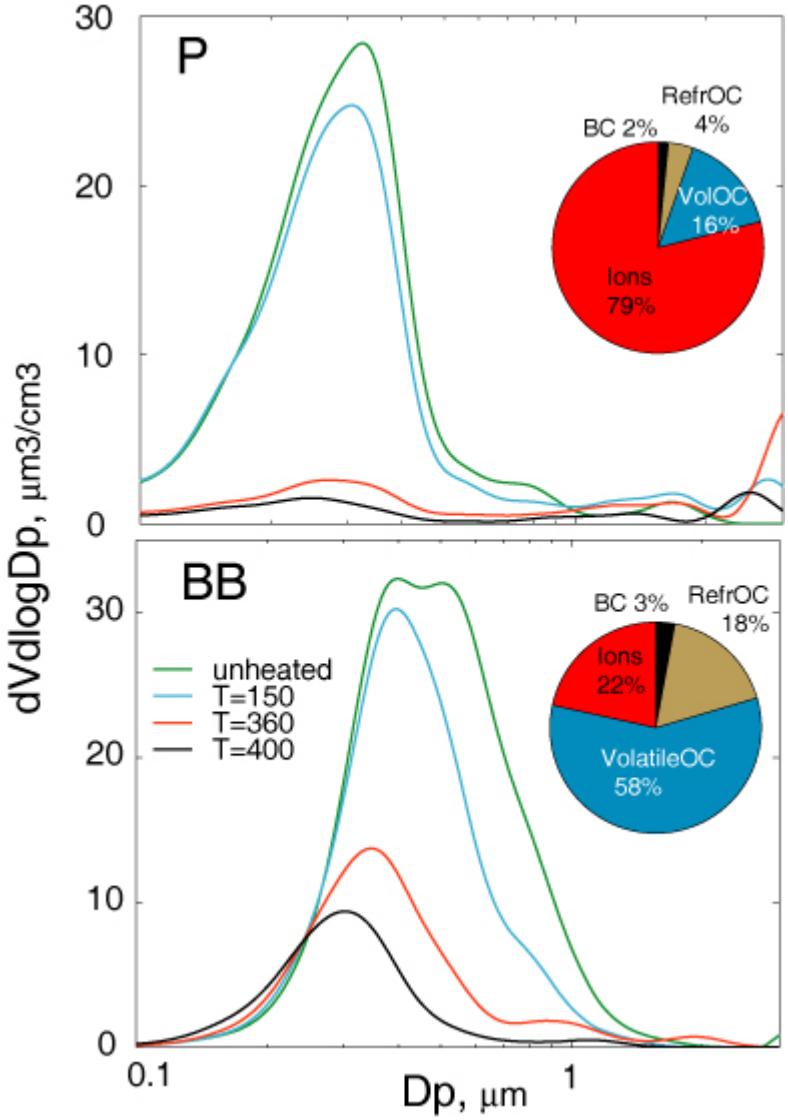

Figure 3. Examples of OPC size distributions with the results of heating aerosol to indicated temperatures for **a)** a pollution plume case and **b)** a biomass burning aerosol case. The mean size and the refractory fraction remaining at 400ºC is much greater for biomass burning aerosol. The pie chart insets illustrate the components described in text.

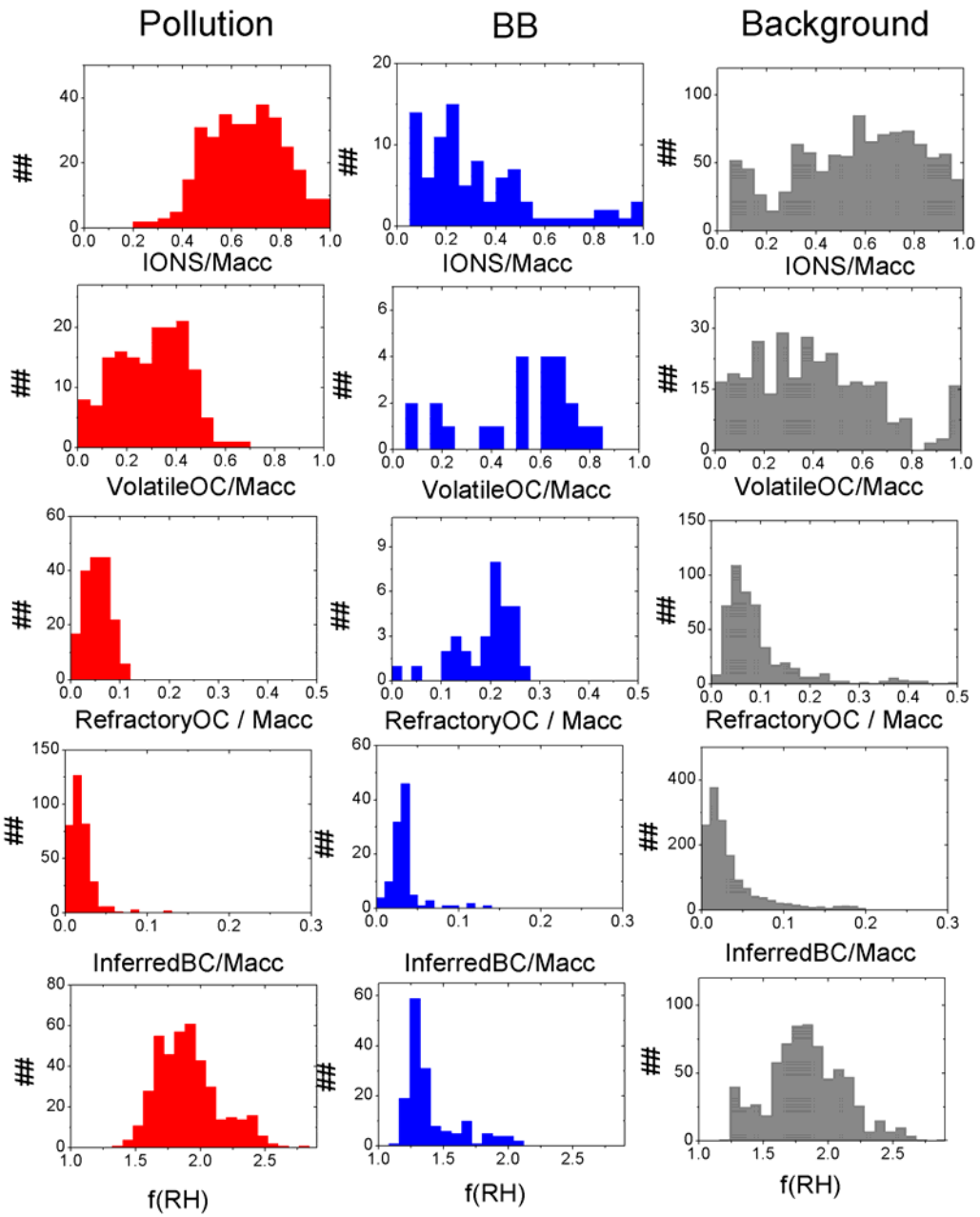

Figure 4. Histograms of mass fractions for the four indicated aerosol components obtained from the analysis described in text for P, BB, and non-plume cases. The lower row includes measured f(RH) associated with these cases.

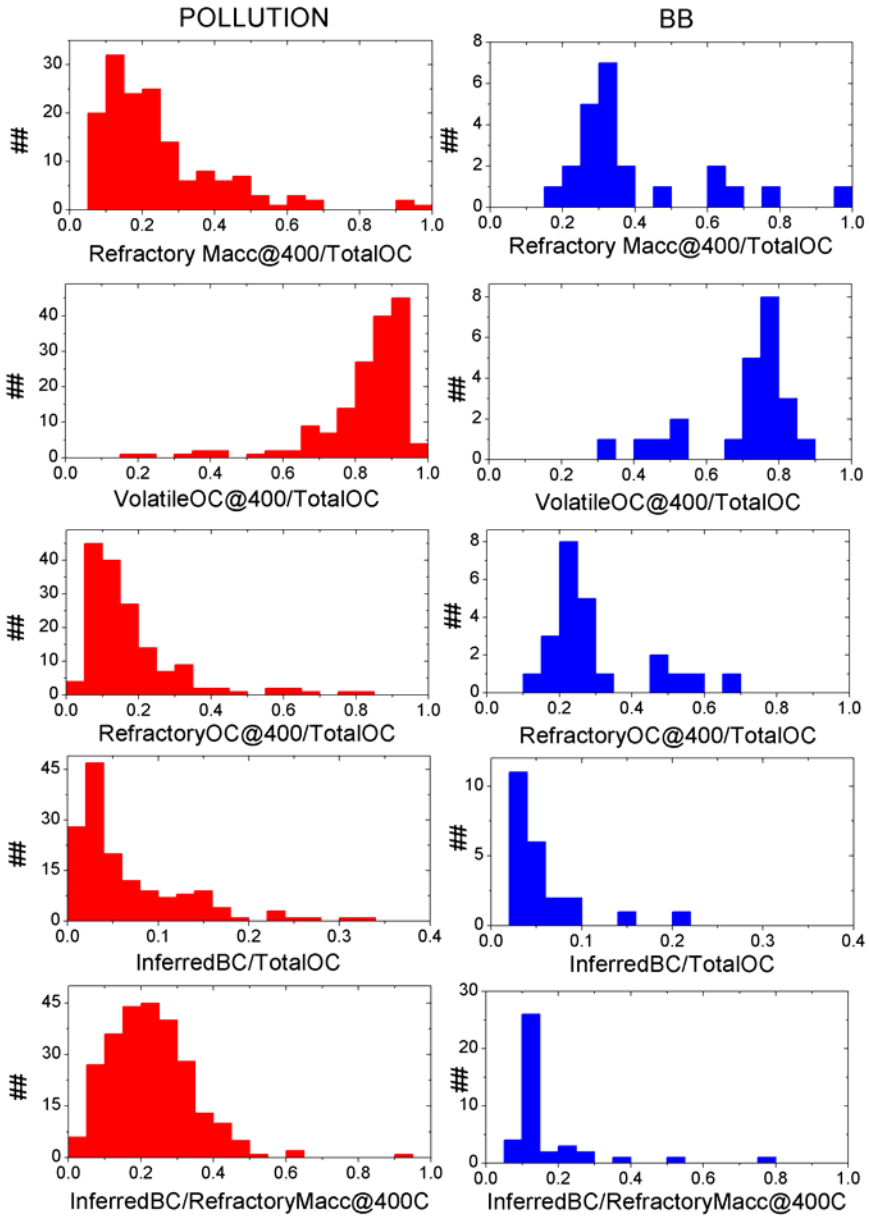

912
913
914
915 **Figure 5.** Histograms for P and BB plumes. From top to bottom these are: Ratio of
916 refractory accumulation mode mass to total OC; the volatile fraction of total OC; the
917 refractory fraction of total OC, the inferred BC mass to OC mass ratio; the inferred BC
918 mass to refractory mass ratio.
919
920
921
922
923

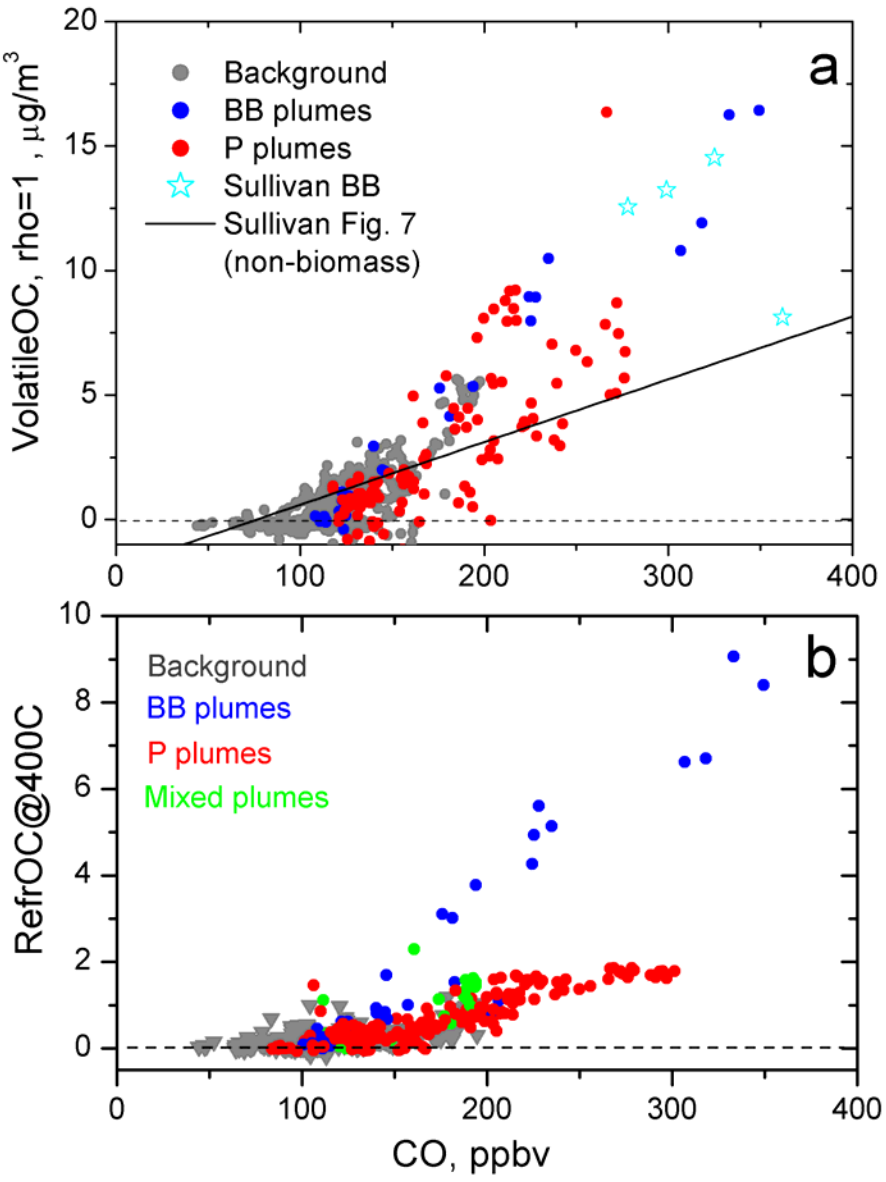

Figure 6. **a)** VolatileOC vs. CO for P, BB and non-plume (background) data converted to unit density by dividing by 1.3 to account for the estimated volatile WSOC non-carbon mass. The regression line for pollution cases only and biomass burning cases (stars) are taken from Sullivan et al. (submitted, see text). The line describes their WSOC (given as µg C m^{-3} for an assumed density of 1.0 g cm^{-3}). Scatter below the zero line (negative VolatileOC) arises at low concentration due to subtraction of distributions (heated and unheated) that are a few minutes apart and provide a measure of uncertainty in this approach. Otherwise all features of the data (scatter, more data above line for higher CO) are the same as seen in the Sullivan et al. WSOC data. **b)** The Refractory OC (ρ = 1.3 g cm^{-3}, this paper) vs. CO shows distinct slopes for P and BB cases.

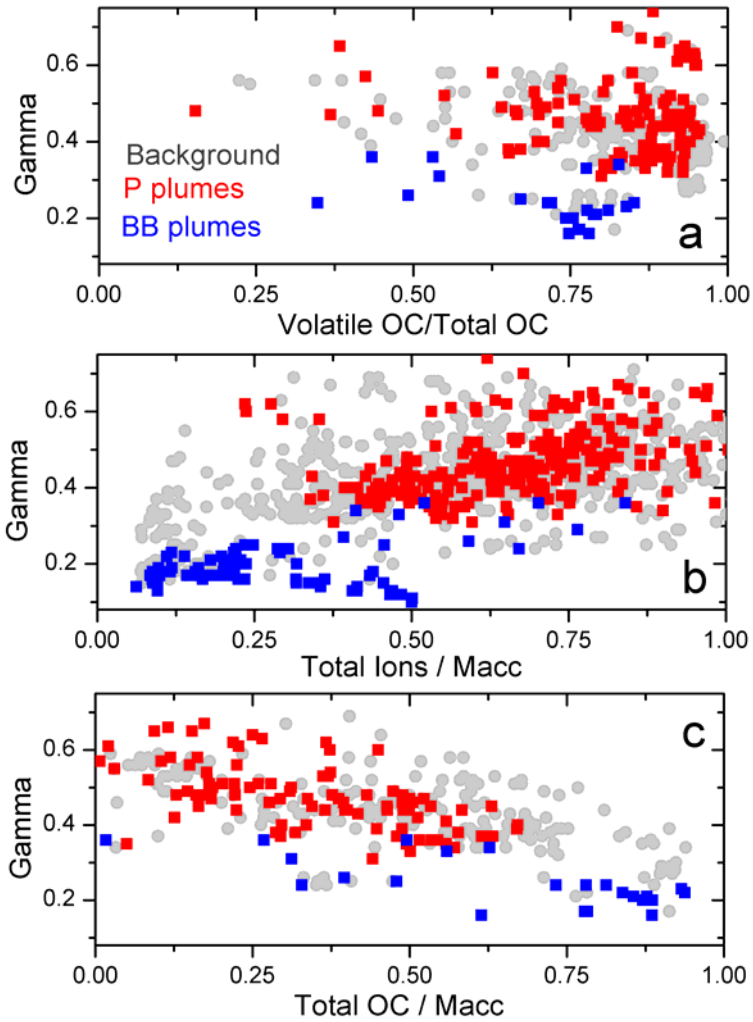

937
938
939
940
941 Figure 7. Plots of gamma (γ) derived from measured f(RH) against **a)** the volatileOC
942 fraction of total OC **b)** the soluble ion fraction of accumulation mode mass and c) the OC
943 fraction of accumulation mode mass.
944
945

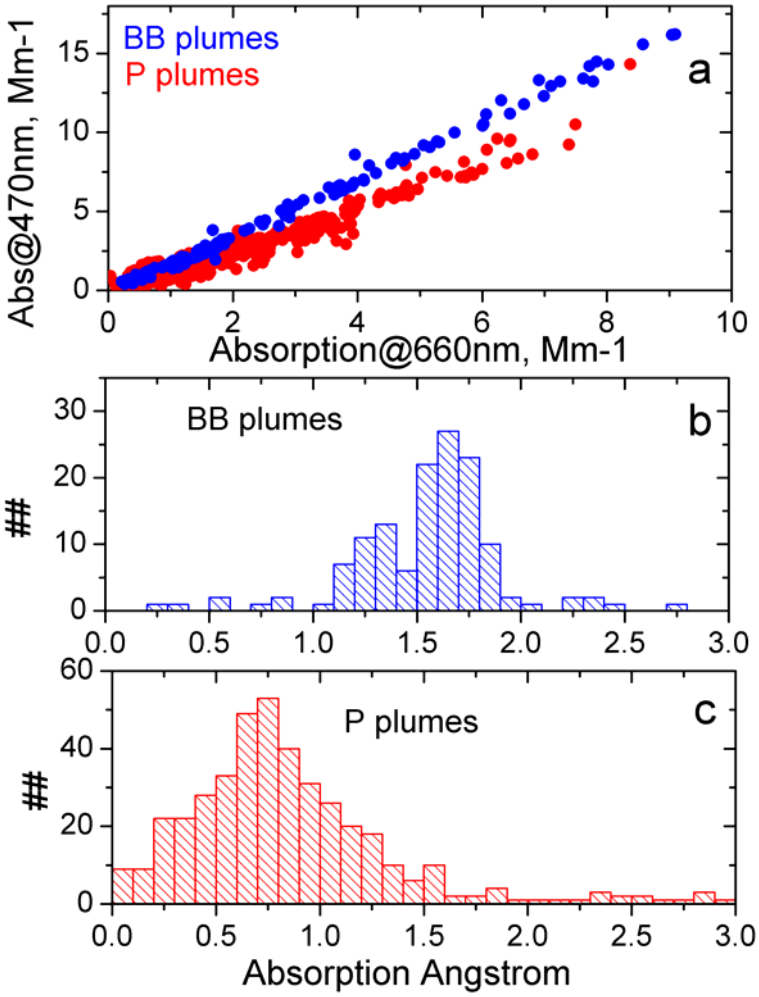

946
947
948 **Figure 8.** **a)** Plot of 3-λ PSAP absorption at 470 nm against 660 nm color coded by B
949 and PP plume identification. Robust wavelenth differences in **b)** and **c)** Angström
950 histograms persist to very low absorption values. The greater variability in the P plume
951 data at lower concentrations reflects more complex varied composition including dust
952 (eg. P points above BB points near origin).
953
954
955

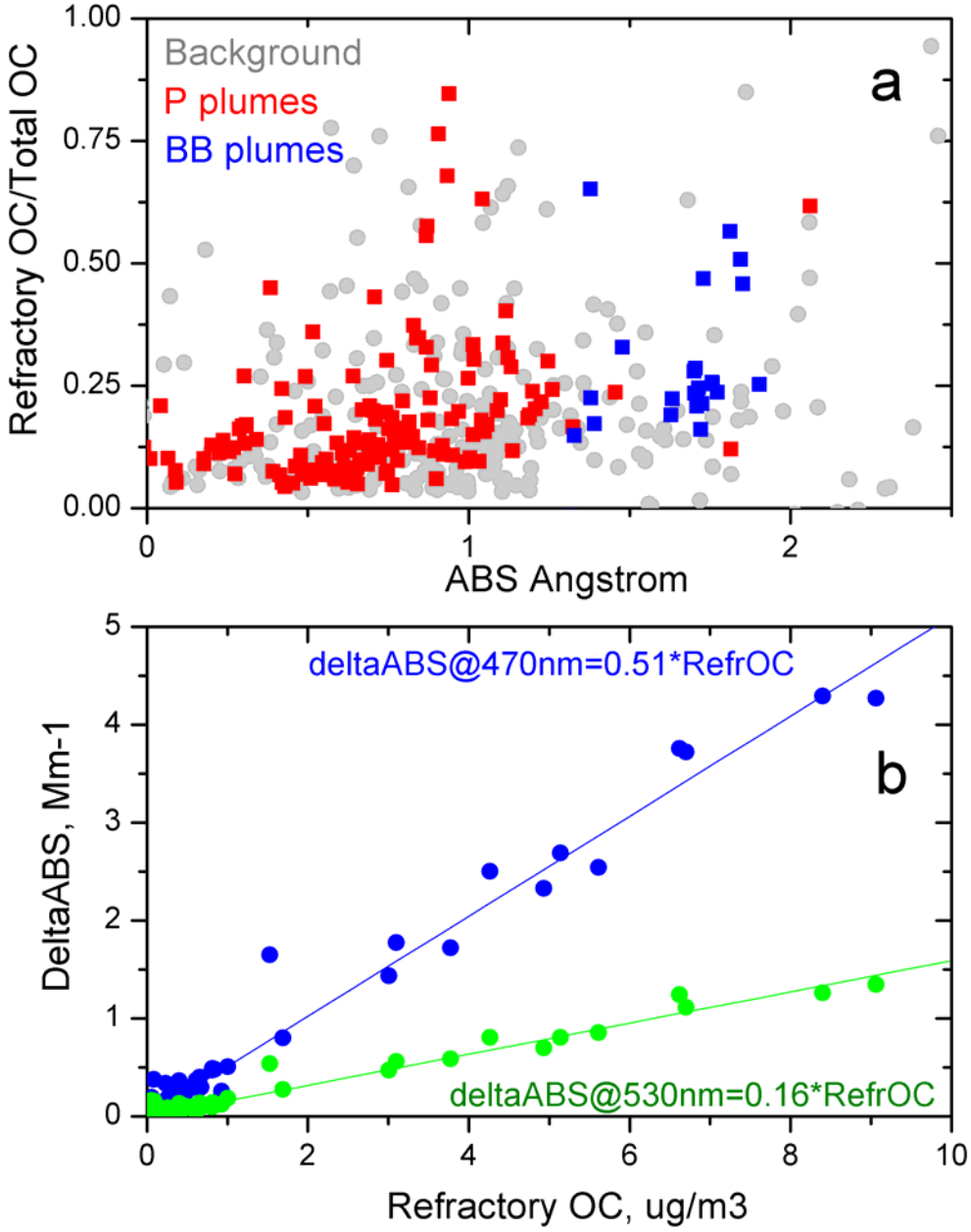

Figure 9. **a)** refractory OC vs. absorption Angström for P, BB and non-plume cases. Higher absorption Angström for BB plumes is clear but also a tendency for this is evident in P and background data. **b)** the non BC absorption enhancement at 470 nm and 530 nm vs. Refractory OC in BB plume have slopes that yield MAE for this component.

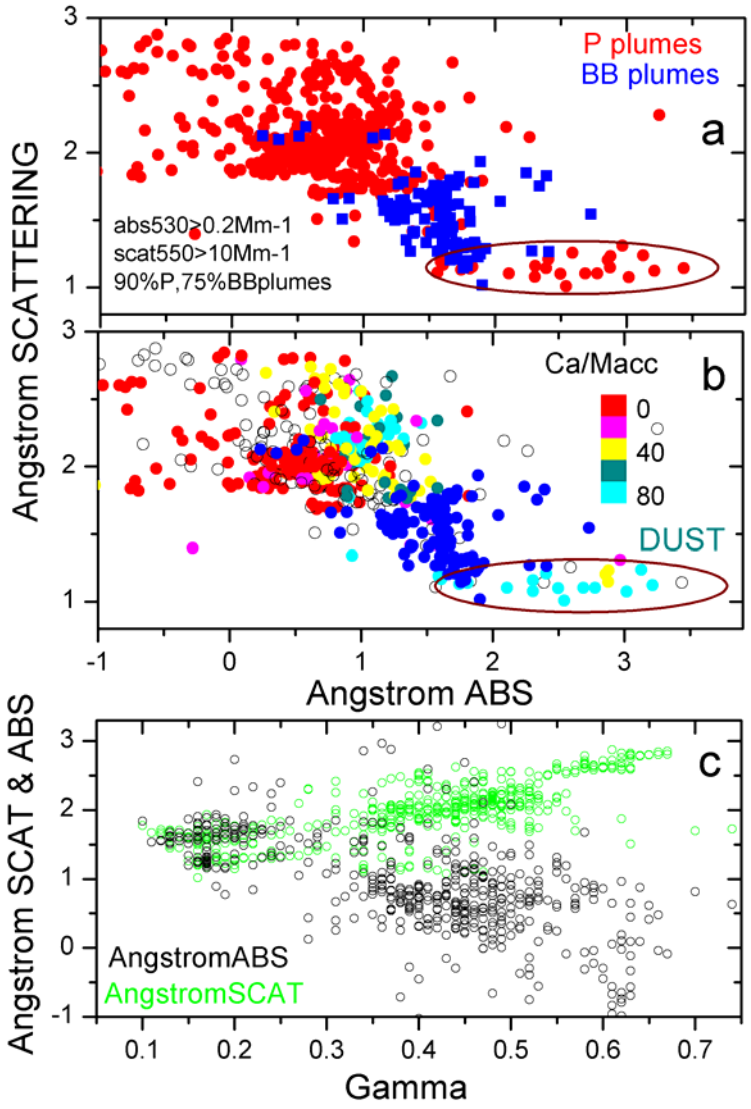

965
966
967 **Figure 10.** **a)** Plot of the wavelength dependence of scattering against the wavelength
968 dependence of absorption for P and BB plumes with anomalous P plumes circled. **b)**
969 same as a) only color coded with Ca/Macc (relative units) revealing dust contributions to
970 anomalous P plumes. **c)** the relationship evident between the scattering and absorption
971 Angström to **γ** indicates coupling of aerosol optics to microphysics and chemistry.
972
973
974
975
976

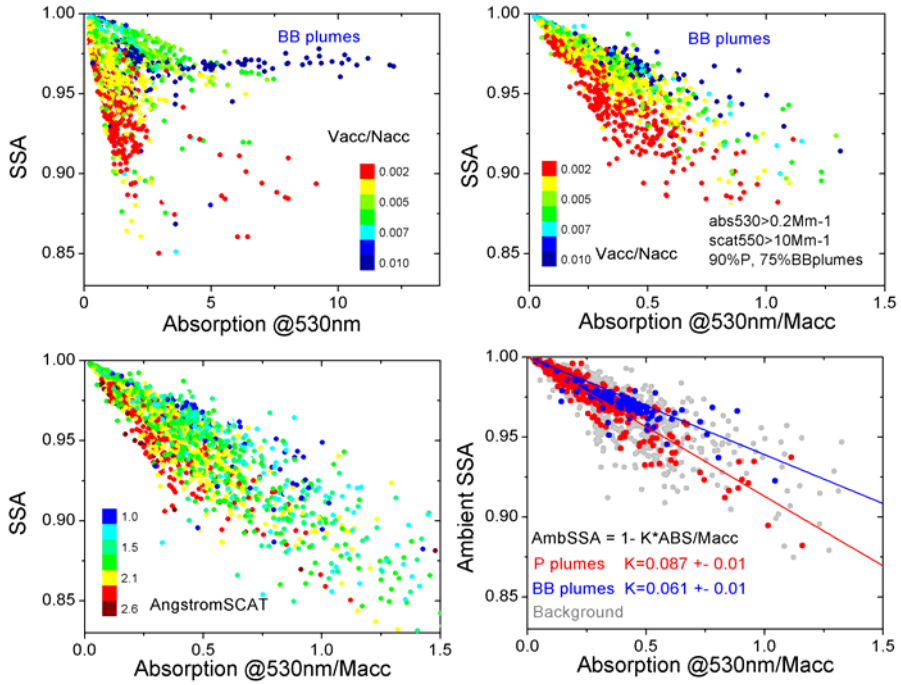

977
978
979 **Figure 11. a)** Dry SSA vs absorption color coded with size parameter, Vacc/Nacc
980 suggests "rainbow" effect. Steeper slopes for smaller sizes (red) indicated a larger
981 absorption to scattering present. **b)** Dry SSA vs. absorption per unit mass reveals
982 stronger "rainbow" with each size parameter showing a strong relationship and a clear
983 effect of size on dry SSA (see text) **c)** Same as b) only color coded with Scattering
984 Angström as a size index and **d)** same as c) only SSA recalculated for ambient humidity
985 and color coded by plume type shows tighter relationship to absorption per unit mass and
986 different regression for P and BB plumes.